Ocean Engineering 287 (2023) 115786

Contents lists available at ScienceDirect

Ocean Engineering

journal homepage: www.elsevier.com/locate/oceaneng

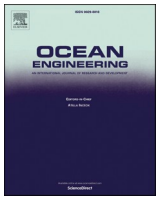

A methodology to calibrate the PICSI cyclic p-y model using experimental results and optimisation

M. Guevara [a,*], J.P. Doherty [b], P.G. Watson [a], D.J. White [c]

[a] Oceans Graduate School, The University of Western Australia, 35 Stirling Highway, 6009, Perth, Australia
[b] School of Civil, Environmental and Mining Engineering. the University of Western Australia, 35 Stirling Highway, 6009, Perth, Australia
[c] School of Engineering. University of Southampton, Burgess Road, Southampton, SO16 7QF, UK

ARTICLE INFO

Handling Editor: Prof. A.I. Incecik

Keywords:
Fatigue analysis
Subsea drilling systems
Whole life model
Soft soils
p-y curves
Conductors

ABSTRACT

Fatigue life estimation of the components of a drilling conductor system is often a critical design consideration. The analysis is usually performed using a coupled system, with the soil-conductor interaction modelled using p-y springs that remain constant throughout the analysis. This means that shifts in bending moment profile that occur due to degradation and recovery of the soil during or after cycling are not accurately modelled. While the PICSI framework (White et al., 2022) can model changes in stiffness and strength of p-y curves due to cycling and pore-pressure dissipation, guidance has not yet been provided on how to calibrate its parameters. This paper presents an experimental methodology for this calibration process based on centrifuge and p-y model testing in reconstituted carbonate silt and kaolin clay. The procedure uses numerical optimisation, and the calibrated parameters are validated against results from an independent set of centrifuge tests on carbonate silt using a flexible pile of similar dimensions to a conductor. It is found that the calibrated model is able to match the changes in cyclic bending moment through a sequence of different packets of cyclic loading. This calibration procedure provides an objective approach for more accurate modelling of conductor fatigue.

1. Introduction

Conductors are the outer-most casing of a drilling system. They prevent the walls of the hole from collapsing and provide axial support for the heavy safety components and inner casings of the system. They are connected to the lower packages (BOP, LMRP) which are in turn connected to the riser system, which is connected to the drill floor, as shown in Fig. 1. When the drilling vessel is impacted by environmental loads, the whole system sways laterally and the embedded riser interacts with the surrounding soil. The behaviour of the soil therefore affects the system response.

Among the various checks that must be performed to ensure a safe drilling operation, fatigue life estimation of the components of the system is often a critical design consideration. Fatigue occurs when repeated stress cycles at specific locations (or hot-spots) produce cracks that could progress to major damage (or failure) of the system. Hot-spots often occur where stress is concentrated, such as discontinuities in the geometry, welds, changes in diameter or thickness, or changes in stiffness such as those produced at the top of cement between the conductor and casing (DNV GL, 2019). Although most hot-spots occur on the wellhead and upper portions of the conductor, some can be located below mudline. Accurate calculation of stress along the length of the conductor and casing string is therefore important for determining the fatigue life of individual system components.

Traditionally, fatigue life is determined by running coupled time-domain analyses of the whole system including the vessel, riser, lower components, conductor, casing and soil. These analyses are performed for a range of seastates that the system will operate in, and the accumulated fatigue from damage in each condition is found to determine the fatigue life. The soil is often modelled using non-linear Winkler springs (using p-y curves) that maintain a constant load-displacement response throughout the analysis. While more refined analysis can be performed by decoupling the system at the lower flex joint (DNV GL, 2019) and modelling the soil as a continuum in a finite element (FE) software, recent experimental studies (Guevara et al., 2022b) have shown that p-y curves can provide an acceptable prediction of bending moment profile.

For monotonic loading, the current API RP 2GEO guidelines (API,

* Corresponding author.
E-mail addresses: mariajose.guevaracastillo@research.uwa.edu.au (M. Guevara), james.doherty@uwa.edu.au (J.P. Doherty), phillip.watson@uwa.edu.au (P.G. Watson), david.white@soton.ac.uk (D.J. White).

https://doi.org/10.1016/j.oceaneng.2023.115786
Received 26 June 2023; Received in revised form 29 August 2023; Accepted 5 September 2023
Available online 3 October 2023

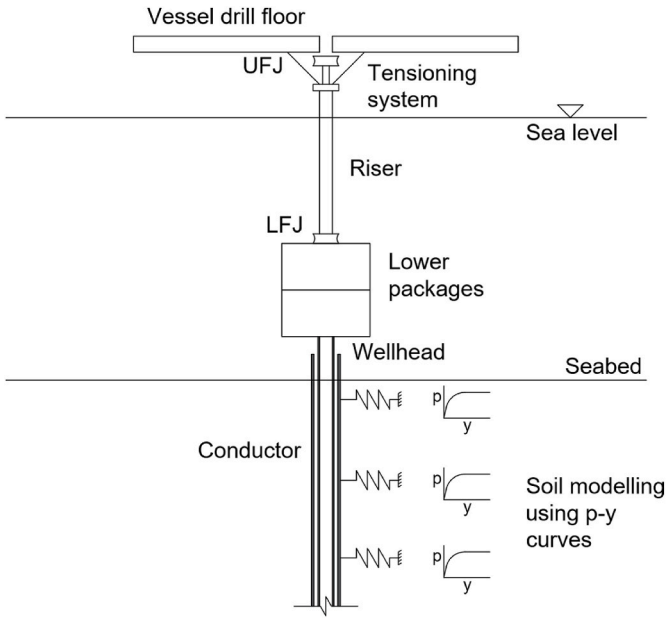

Fig. 1. Modelling lateral soil-conductor interaction with p-y curves.

2014) recommend p-y curves that are widely acknowledged to under-predict the lateral stiffness at small displacements (Jeanjean, 2009). Typical operational displacements for conductors are below 10% of the conductor diameter (d) and are therefore in the range where the API curves do not predict the stiffness accurately. More recent studies (Jeanjean et al., 2017) have proposed p-y curves that reflect the observed results from centrifuge tests and databases of field experience. These studies are being incorporated in the draft ISO 19901–4 (ISO/DIS, 2021) with certain modifications to the p-y curves. Other authors have also proposed methods of constructing monotonic p-y curves based on scaling from laboratory simple shear test results (Bransby, 1999; Zhang and Andersen, 2017).

Since the environmental loading on a drilling conductor system is cyclic, monotonic p-y curves are unlikely to adequately capture the changes that occur in the soil-conductor stiffness over the operational life of the system, and other (recent) approaches have therefore been proposed to model this scenario. One approach relies on the accumulation of pore pressures from different amplitude cycling loading to determine a factor by which the monotonic curve must be modified (Zhang et al., 2017). Other authors (Zakeri et al., 2019) propose methods for estimating a characteristic "steady-state" (cyclic) stiffness that is assumed to be reached after a several hundred cycles, with this method originally developed based on observations from centrifuge testing in kaolin clay and Gulf of Mexico clay (Zakeri et al. 2016a, 2016b), as well as p-y apparatus tests (Zakeri et al., 2017) on other types of clay. A recent method (Komolafe and Aubeny, 2020) extends the "steady state" stiffness approach by modelling the transition from undisturbed stiffness to the fully remoulded state, for the range of displacements expected to be experienced by drilling conductors. However, none of these approaches can model the impact of the entire load history on soil-conductor stiffness on a time-domain type of analysis, transitioning from undisturbed to remoulded to reconsolidated.

Previous studies for steel catenary risers (Hodder et al., 2009; Sahdi, 2013), lazy wave risers (Safaqah et al., 2022) and pipelines (Hou, 2020) have shown the impact of load history on soil-pipe stiffness through episodes of cycling and consolidation, whereby an initial loss of stiffness is then regained (after cycling stops) due to pore pressure dissipation. Furthermore, these studies have also demonstrated that a regain in stiffness and strength can be achieved while cycling, provided the rate of pore pressure dissipation and recovery exceeds the rate of damage induced by remoulding. Similar changes in stiffness have been observed in laterally loaded short piles from experimental studies in centrifuge. Here, the regain in stiffness and strength due to episodic loading followed by consolidation periods was documented for laterally loaded piles in kaolin clay by Zhang and Randolph (2011), and in reconstituted carbonate silt by Doherty et al. (2019). Moreover, an increase in soil-pile stiffness was found to occur during cycling by Guevara et al. (2020) for tests with large numbers of cycles ($N > 10{,}000$). Guevara et al. (2020) also report a higher regain in stiffness from continuous cyclic loading when compared to multiple (short) episodes of loading with consolidation periods in between, to achieve the same overall timeframe. This observation is comparable to that documented by Hou (2020) for steel catenary risers, suggesting that in soft soils, the more pore pressure that is generated through remoulding, the higher the subsequent densification that can occur – leading to a greater potential regain in stiffness. Furthermore, based on centrifuge tests of rigid piles in reconstituted carbonate silt and kaolin clay, Guevara et al. (2020, 2022b) demonstrated that the sequencing of cyclic loading is important. These studies showed that large amplitude cycling can significantly reduce the strength and stiffness in subsequent smaller amplitude cycles, compared to the strength and stiffness applicable if the large amplitude cycling had not occurred.

Aside from model testing, the effects of load-history have been observed through multiple episodic simple shear tests on kaolin clay (Laham et al., 2021) and multiple amplitude partially drained cyclic triaxial tests in sand (Jostad et al., 2021).

Frameworks have previously been proposed to model the effect of episodes of cyclic loading and consolidation on soil strength and stiffness for different applications (White and Hodder, 2010; Zhou, 2019). These model the effects of remoulding and consolidation as separate processes and capture the corresponding changes in bearing capacity. Building on these models, White et al. (2022) recently proposed a method (PICSI) to model the p-y response of laterally-loaded piles, with the p-y spring being continuously updated based on the effects of load history, inspired by traditional critical state soil mechanics (Wood, 1990), and with additional features observed from centrifuge tests. This method allows for remoulding and consolidation to occur in parallel, with the p-y spring updated accordingly. While some examples of its application were given, no guidance was provided on how the PICSI model could be calibrated. Accordingly, this paper describes a method for calibrating the model based on experimental (centrifuge and p-y apparatus) test results. It is acknowledged that these tests are not routinely performed, and an alternative strategy would be to develop methods to derive these parameters from simple shear or triaxial tests, which are more commonly performed as part of site characterisation activities. In addition to the calibration method, this paper presents a modification to the original PICSI formulation, which led to a reduction in the number of model parameters to calibrate.

2. The PICSI framework

The Parallel-Iwan Critical-State Inspired (PICSI) model proposed by White et al. (2022) tracks soil softening produced by lateral displacement of a pile, as well as hardening caused by the dissipation of the excess pore pressure. The p-y model consists of two components.

- A parallel Iwan (PI) model (Iwan, 1966) for the hysteretic non-linear p-y response, which consists of parallel springs and sliders (Fig. 2).
- A critical state-inspired (CSI) model for hardening and softening of the p-y response.

The net effect of the softening (damage) and hardening varies with time and is used to scale the spring stiffness (k_i) and slider capacities (s_i) within the Parallel-Iwan model (Fig. 2).

The model uses an analogue of the void ratio – strength relationship that underlies critical state soil mechanics, with additional features to replicate observations from model tests. The void ratio is replaced with a

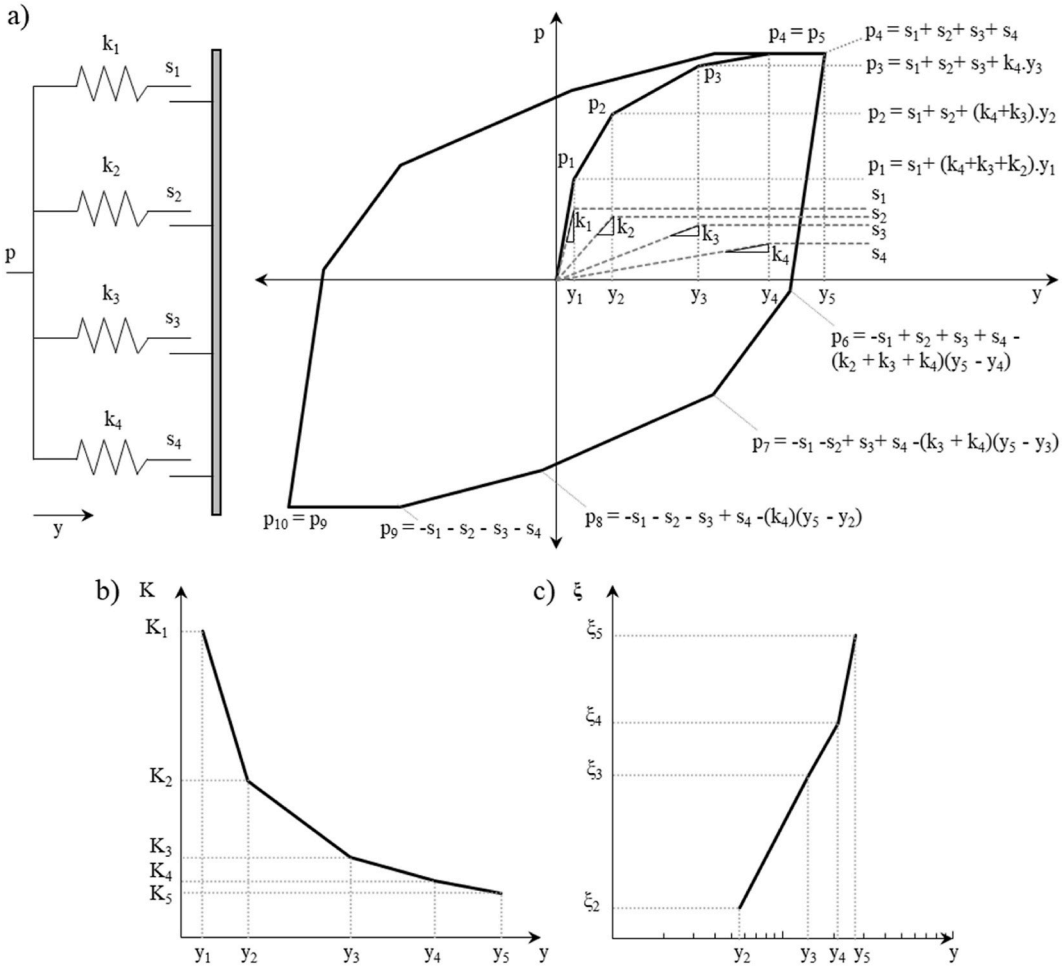

Fig. 2. A) Parallel-Iwan arrangement of springs and sliders of stiffness k_i and capacity s_i, b) secant stiffness (K) of PI model vs amplitude, c) damping ratio (ξ) of PI model vs amplitude.

hardening index H, and the mean effective stress is replaced by the undrained shear strength normalised by the initial strength, $s_u/s_{u,i}$. Fig. 3a shows envelopes of the attainable states of strength and hardening. The shape of the lower portion of the envelope depends on the equation chosen to describe it.

The damage, D, is caused by shearing of the surrounding soil when the pile is displaced laterally, y, and cannot exceed D = 1, which is shown in Fig. 3 as the lower-left envelope and is analogous to the critical state line (CSL) (Wood, 1990). Damage recovers with time due to pore pressure dissipation (consolidation). The function that describes the incremental change of damage δD for a normalised displacement (δy/d) and time increment δt is:

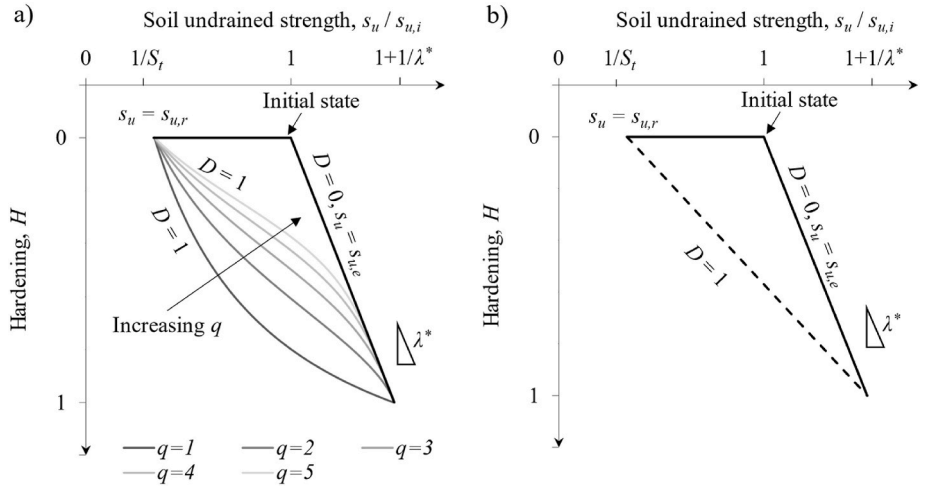

Fig. 3. Model strength envelopes: a) original formulation, and b) modified formulation.

$$\delta D = d_r(1-D)^{d_p}\left|\frac{y}{y_{ref}}\right|^{d_a}\left|\frac{\delta y}{d}\right| - c_r\left(\frac{c_v}{d^2}\right)D^{c_p}\delta t \quad (1)$$

The equation consists of two parts.

- The first part corresponds to the increase in damage produced by a given normalised displacement increment (δy/d). Damage also depends on the absolute displacement (y) normalised by the peak displacement (y_{ref}), as well as the current accumulated damage (D). Fitting parameters d_r, d_p and d_a enable the relative contribution of these components to be adjusted in the calibration process.
- The second part of the equation corresponds to recovery from damage through the dissipation of excess pore pressures, which is dependent on the coefficient of consolidation (c_v), the conductor diameter (d), and parameters that control the rate of recovery c_r and c_p.

The densification of soil due to the dissipation of the pore pressures generated during cycling is modelled by the hardening index, H. Note that the model was developed for soils that tend to densify when sheared, i.e. soils that lie to the right of the critical state line. The variation in hardening with time can be described with the following equation:

$$\frac{\delta H}{\delta t} = c_r(1-H)^{h_p}\left(\frac{\kappa^* c_v}{d^2}\right)D^{c_p} \quad (2)$$

The current level of hardening will depend on accumulated damage, the consolidation parameters c_r and c_p, the coefficient of consolidation of the soil (c_v), and the hardening parameters h_p and κ*.

The current normalised strength ($s_u/s_{u,i}$) depends on the current levels of hardening (H) and damage (D). An equilibrated strength ($s_{u,e}$) is defined as the strength at the current H when D = 0:

$$\frac{s_{u,e}}{s_{u,i}} = 1 + \frac{H}{\lambda^*} \quad (3)$$

The current strength (s_u) is therefore:

$$\frac{s_u}{s_{u,e}} = 1 - D\left(1 - \frac{1}{S_t}\right) \quad (4)$$

A general form of the model (Fig. 3a) allows soil sensitivity to vary with hardening, from $S_t = S_{t0}$ at H = 0 to $S_t = 1$ at H = 1, at a rate set by the power, q:

$$S_t = 1 + (S_{t0} - 1)(1-H)^q \quad (5)$$

In this paper, a simplification is proposed for calculating the soil sensitivity by assuming the D = 1 envelope varies linearly with hardening, plotted as the dashed line in Fig. 3b. This can be achieved by replacing equation (5) with the following equation, with the model then independent of the parameter q:

$$S_t = \frac{S_{t0}(H+\lambda^*)}{\lambda^*(1-H) + S_{t0}H(\lambda^*+1)} \quad (6)$$

As will be shown in following sections, this simplification provides acceptable agreement with the data, while reducing the number of parameters needed to be calibrated. It is important to note that although some tests reached a large number of cycles (N ≈ 20,000), the strength appears to continue increasing rather than reaching a plateau (as it would when H → 1). This implies that more cycles would be needed to fully calibrate the model, and as such the simplification proposed in this paper (as well as the calibrated parameter λ*) represents only a first approximation – which may be updated in future using tests where H = 1 (i.e. $s_{u,r} = s_u$).

Another important aspect to note in the PICSI model is that by formulating the recovery from damage as per White et al. (2022), the strength will always be higher than the initial strength once pore pressures induced by cyclic loading have fully dissipated. This is a good approximation for materials for which soil structure, ageing and cementation between particles do not play a large role in the sensitivity of the soil. For soils where these aspects are important, it may be possible to model these by introducing a 'non-recoverable strength' term, such as through modification of equations (3)–(5) or (6). This is the subject of further work, requiring testing of undisturbed natural soils.

Implementation of the model is performed via a sequential analytical process, documented more fully in White et al. (2022). Fig. 4 shows the procedure at a spring level when subjected to a time-history of displacements (y(t)) – and it is observed that at each time-increment (δt), the strength and stiffness of the parallel-Iwan system is affected by both the current level of damage D and hardening H produced by the time history of displacement.

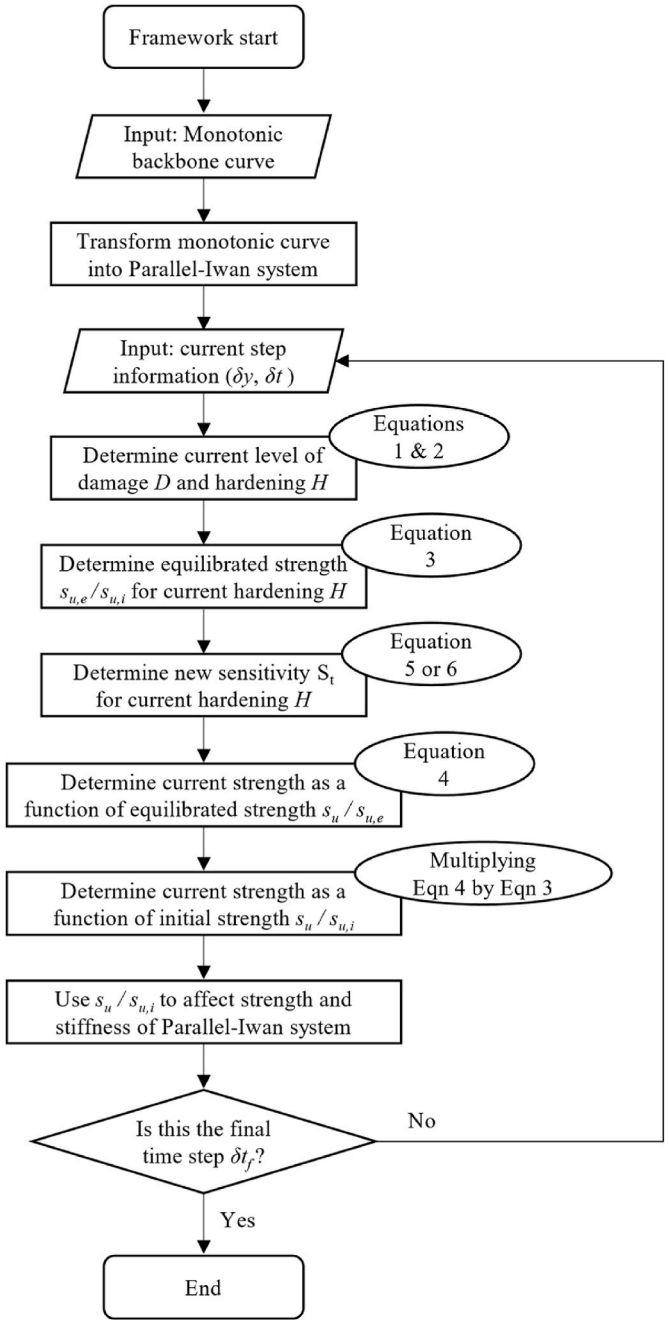

Fig. 4. Framework procedure at a p-y spring level.

3. Experimental data

Physical modelling was performed to observe key aspects influencing the stiffness of soil-conductor lateral behaviour, and to calibrate the PICSI model parameters. Details on the observations derived from the centrifuge and p-y apparatus tests can be found in Guevara et al. (2020, 2022b; c). From these tests the horizontal forces/pressures and displacements with time were extracted to calibrate the model by tracking changes in normalised cyclic secant stiffness (K), defined as:

$$K = \frac{\Delta p / p_u}{\Delta y / d} \tag{7}$$

where Δp is the cyclic range of horizontal pressure; p_u is the measured lateral capacity from a monotonic test; d is the pile diameter; and Δy is the range of lateral displacement (peak to peak).

3.1. Soil characterisation

Two different reconstituted samples were used for the tests described in this paper: a carbonate silt recovered from offshore Australia (Chow et al., 2019) and UWA kaolin clay (Stewart, 1990). The properties of carbonate silt and kaolin clay were obtained through laboratory classification and element tests in accordance with relevant Australian and ASTM standards, and are summarised in Table 1.

Samples for element testing were reconstituted with moisture content (w) of 140% for the carbonate silt and 130% for the kaolin clay, roughly twice the liquid limit. The slurry was then consolidated in tubes under a vertical pressure representing an embedment depth of 6.0 m for the carbonate silt (30 kPa) and 11.0 m for the kaolin clay (65 kPa). The vertical stress was selected to ensure that a sample with strength (s_u) of 10 kPa would be produced, as this was needed for handling and placing the samples in the p-y apparatus. The soil strength gradient (s_u/σ'_{v0}) and increase in strength due to rate effects were determined via CK_0U simple shear tests at slow and fast rates. Cyclic T-bar penetrometer tests were also performed on the centrifuge samples to measure soil strength gradient with depth ($k_{T\text{-}bar}$) and sensitivity, derived using a capacity factor $N_{T\text{-}bar} = 10.5$ (Stewart and Randolph, 1991). Profiles of moisture content, unit weight, undrained shear strength from T-bars and monotonic simple shear tests are presented in Fig. 5.

It is observed from Fig. 5a and **b** that the extrapolation of the T-bar strength gradient with depth coincides with the slow simple shear tests, despite the T-bars being performed at higher strain rate than the slow simple shear tests. This is thought to relate to partial soil softening induced during initial penetration of the T-bar offsetting the increase due to the loading rate (Einav and Randolph, 2005; Zhou and Randolph, 2009a, 2009b).

Table 1
Properties of tested Kaolin clay and Carbonate silt.

Description	Parameter	Carbonate Silt	Kaolin Clay
Undrained shear strength gradient (from CK_0U SS tests sheared at 22%/h)	s_u/σ'_{v0}	0.32	0.22
Sensitivity (from cyclic T-bar tests)	S_t	3.3	2.4
Specific Gravity	G_s	2.76	2.6 (Boukpeti et al., 2012)
Increase in strength due to rate effects		18% per log cycle	9% per log cycle
Operative coefficient of consolidation	c_h	1 m^2/year (consistent with Chow et al., 2019)	3.3 m^2/year (consistent with Richardson et al., 2009)
Plastic Limit	LL	63	61 (Stewart, 1990)
Liquid Limit	LP	42	27 (Stewart, 1990)
T-bar strength gradient with depth	$k_{T\text{-}bar}$	1.65 kPa/m	1.05 kPa/m

3.2. Centrifuge tests

Centrifuge testing involved the laterally translation of a rigid pile installed in reconstituted normally consolidated samples of kaolin clay and carbonate silt at 40 g. The moisture content (w) of each slurry was the same as for samples consolidated for element testing, as described in the previous section. The tests were conducted in the 1.8 m radius beam centrifuge at the National Geotechnical Centrifuge Facility, University of Western Australia. The experimental setup is shown in Fig. 6 and more details can be found in Guevara et al. (2021).

The model pile was 3D printed in stainless steel to represent a prototype conductor with a diameter of 780 mm (30 inch) and a wall thickness of 38 mm (1.5 inch). The pile was connected to a bending leg, which was used to determine the lateral load (F_h) applied to the conductor. The displacement and rotation of the pile were measured using two lasers and a flat plate bracket as a target. The hollow pile was installed in flight by monotonic jacking. Test locations were separated by at least 6 pile diameters from each other and the walls of the box to avoid interaction between tests.

The tests were displacement controlled at the actuator level to best represent the nature of the loading from a floating drilling vessel, and the pile can be considered rigid for the range of loading applied. Based on the rigidity criteria proposed by Poulos and Hull (1989), the pile is considered rigid for the range of loading applied (critical length >3 times the pile length). The test sequences are described in Table 2 and Table 3 for the carbonate silt and the kaolin clay, respectively. The amplitudes at mid-depth are expressed in terms of half the range of normalised lateral displacement (i.e. half of the peak to peak amplitude) $\Delta y/2$ d.

Generally, each test comprised episodes of cyclic loading with pore pressure dissipation (pause) periods in between, with each episode comprising a packet of cycles of constant amplitude. The frequency and number of cycles of loading within an episode was selected to ensure that each episode was effectively undrained (≤25% dissipation), which was estimated using the Osman and Randolph (2012) dissipation solution. Using the same approach, the period between episodes was set to ensure ≈75% dissipation of the pore pressures generated in the last episode. This percentage was later compared with the data from the pore pressure sensors on the pile and found to be around 76% for the kaolin clay tests, and 65% for the carbonate silt. The packet sequence increases and decreases in amplitude symmetrically with respect to the largest amplitude packet.

Although aiming for pure lateral translation, the presence of the load cell and connection pieces created a very small compliance in the loading system. This was accounted for by developing a relationship between the applied load and the pile rotation (measured with the two lasers), which was then used to determine the lateral displacement at 50% of the pile tip depth. The integrated response of the distributed soil pressure (p) along the length of the pile was determined via the measured lateral load (F_h) and the projected embedded portion of the pile (i.e F_h/dL). The lateral displacement at mid-embedment depth ($\Delta y/d$) and the pressure measured on each cyclic test (Δp), along with the ultimate pressure measured from the monotonic push (p_u) were then used to determine the normalised secant stiffness (K) during each cycle. It should be noted that the measured lateral load includes contributions from both (near surface) wedge and (deeper) flow around mechanisms. A contribution also occurs due to shearing at the base of the pile, although this is small and can be ignored. A discussion is presented in the results section on how this might impact the calibration of the model.

3.3. p-y apparatus tests

The p-y apparatus tests were performed in Norway using equipment

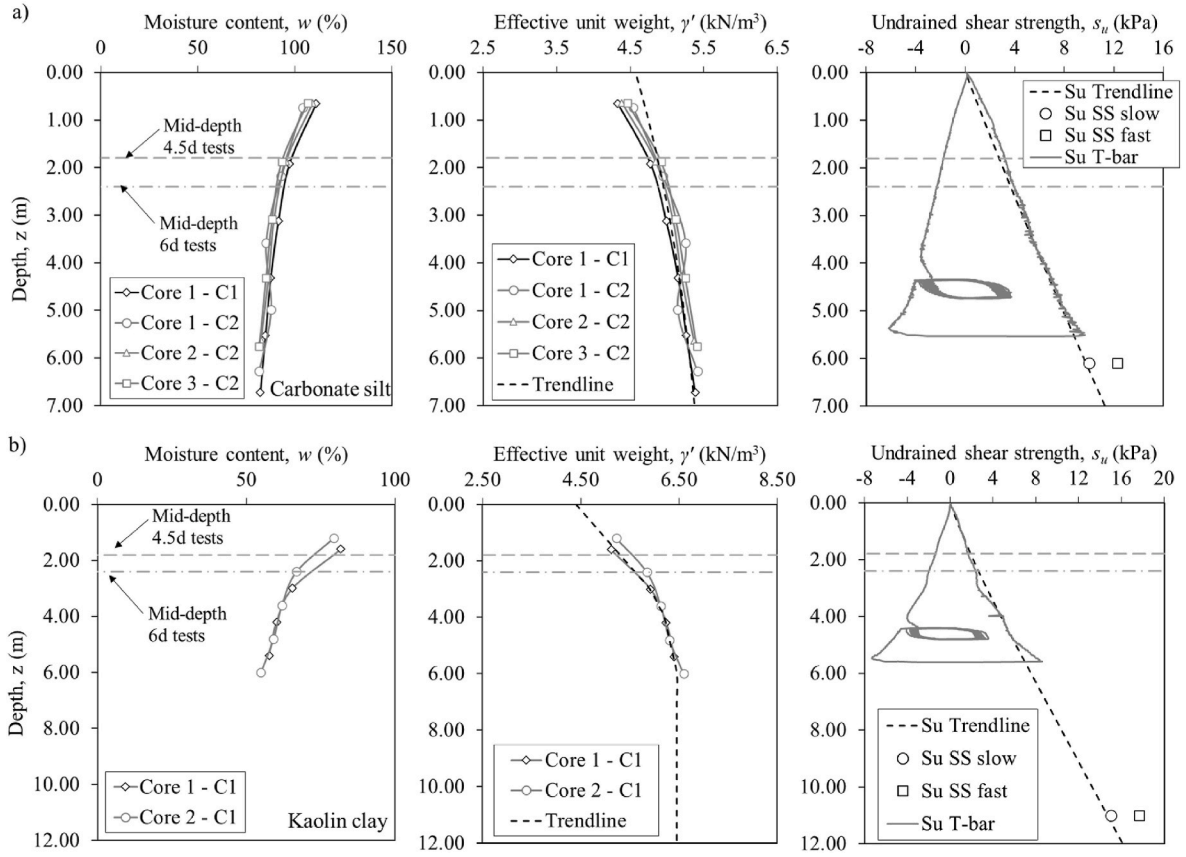

Fig. 5. Moisture content, effective unit weight and undrained shear strength profiles for First (C1) and Second (C2) Campaigns for both a) Carbonate silt and b) Kaolin clay.

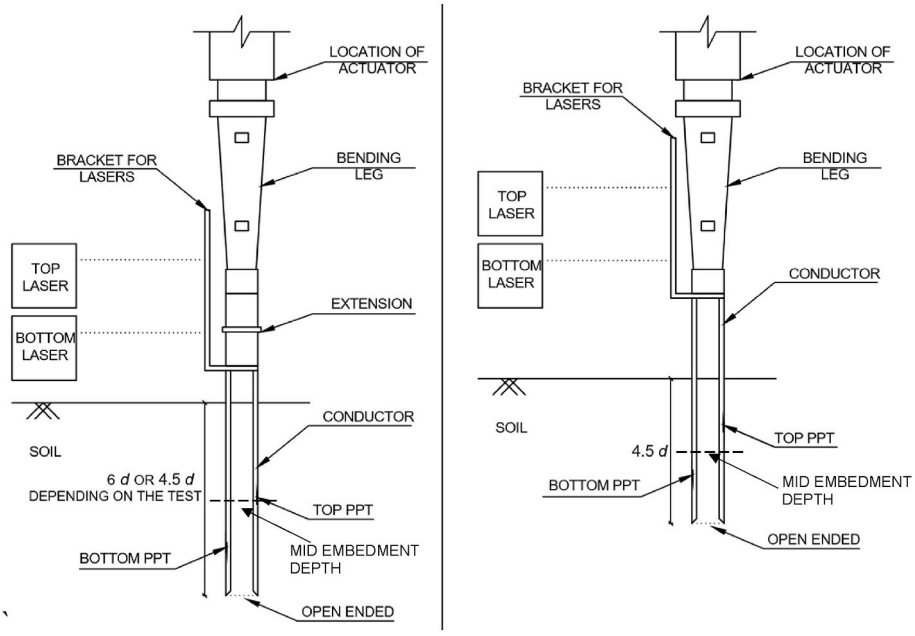

Fig. 6. Diagram of test setup: (a) First campaign setup, (b) Second campaign setup. From Guevara et al. (2020).

designed by BP and operated by NGI (Zakeri et al., 2017), using samples consolidated from slurry in tubes and with an internal diameter of 72 mm. The consolidation pressures applied in preparing the samples were the same as those used for element testing. The p-y apparatus uses a 10 mm diameter rod inserted in a pre-augered hole in a sample with height-to-width of between 1:1 and 2:1. The sample was consolidated with end plates on both ends from which the inserted rod protrudes. Once the sample is consolidated in the apparatus, the rod is moved laterally while maintaining constant volume/height with the end plates. The consolidation pressures adopted for testing were 3 kPa greater than

Table 2
Centrifuge test sequences – carbonate silt.

Test number	Embedment Depth	Amplitude at mid-depth, Δy/2 d (−)	# of cycles (N) per packet of amplitude	Number of episodes
CS1 (1st Campaign)	4.5 d and 6.0 d	Monotonic push	–	1
CS2 (2-way loading) (1st Campaign)	4.5 d and 6.0 d	Packet 1: 0.0006 Packet 2: 0.0009 Packet 3: 0.0022 Packet 4: 0.0059 Packet 5: 0.0144 Packet 6: 0.0284 Packet 7: 0.037 – PF Packet 8: 0.038 – PF Packet 9: 0.039 Packets 10 to 18: symmetrically "unloaded" via matching cyclic packets.	150	1
CS3 (2-way loading) (1st Campaign)	4.5 d and 6.0 d	Packet 1: 0.0035 Packet 2: 0.0113 Packet 3: 0.0346 Packet 4: 0.0186 Packet 5: 0.0087	100	4
CS4 (1-way loading) (1st Campaign)	4.5 d and 6.0 d	Packet 1: 0.005 Packet 2: 0.0183 Packet 3: 0.0669 Packet 4: 0.0320 Packet 5: 0.0130	200	4
CS5.1 (2-way loading) (2nd Campaign)	4.5 d	Packet 1: 0.0205 Packet 2: 0.03 Packet 3: 0.024	200 (small amplitude), 2 (larger amplitude)	2
CS5.2 (2-way loading) (2nd Campaign)	4.5 d	Packet 1: 0.022 Packet 2: 0.033 Packet 3: 0.023	200 (small amplitude), 20 (larger amplitude)	8
CS5.3 (2-way loading) (2nd Campaign)	4.5 d	Packet 1: 0.019 Packet 2: 0.042 Packet 3: 0.028	200 (small amplitude), 200 (larger amplitude)	2
CS6 (2-way loading) (2nd Campaign)	4.5 d	0.05	200	9
CS7 (2-way loading) (2nd Campaign)	4.5 d	0.048 to 0.029	10,000	2
PF: Monotonic Push forward 0.10 d				

Table 3
Centrifuge test sequences - kaolin clay.

Test number	Embedment Depth	Amplitude at mid-depth, Δy/2 d (−)	# of cycles (N) per packet of amplitude	Number of episodes
KC1 (1st Campaign)	4.5 d and 6.0 d	Monotonic push	–	1
KC2 (2-way loading) (1st Campaign)	4.5 d and 6.0 d	Packet 1 and 2: 0.0009 Packet 3 and 4: 0.0091 Packet 5: 0.0217 Packet 6: 0.035 – PF Packet 7: 0.035 – PF Packet 8: 0.035 Packets 9 to 15: symmetrically "unloaded" via matching cyclic packets.	150	4
KC3 (2-way loading) (1st Campaign)	4.5 d and 6.0 d	Packet 1: 0.0057 Packet 2: 0.0209 Packet 3: 0.0459 Packet 4: 0.0220 Packet 5: 0.0115	100	4
KC4 (1-way loading) (1st Campaign)	6.0 d	Packet 1: 0.0033 Packet 2: 0.0210 Packet 3: 0.0687 Packet 4: 0.0296 Packet 5: 0.0111	200	4
PF: Monotonic Push forward 0.10 d				

Table 4
P-y apparatus test sequences – carbonate silt and kaolin clay.

Test number	Amplitude, Δy/2 d (−)	# of cycles (N) per packet of amplitude	Number of episodes
CS1_py and KC1_py (2-way loading)	0.04–0.08 – 0.04	250 (small amplitude), 25 (larger amplitude)	3
CS2_py and KC2_py (2-way loading)	0.04–0.08 – 0.04	250 (small amplitude), 250 (larger amplitude)	3
CS3_py and KC3_py (2-way loading)	0.35	100	1
CS4_py and KC4_py (2-way loading)	0.0004–0.002 – 0.009–0.04 – 0.009–0.002 – 0.0004	100	1

the pressures used during sample preparation, in order to minimise potential disturbance of the prepared samples due to transportation from Perth to Norway. The test sequences applied in the p-y apparatus for the carbonate silt and kaolin clay samples are shown in Table 4.

The applied displacement (Δy/2 d) and measured pressure (Δp) on the rod, along with the ultimate pressure (p_u) from the respective large amplitude monotonic tests (CS3_py and KC3_py), were then used to determine the normalised secant stiffness (K) during each cycle (Equation (7)). The pressure from the first peak of the monotonic push test is used to normalise the stiffness results from cyclic testing, which is the most straightforward choice of ultimate pressure for normalising the p-y apparatus tests results. However, as discussed in Guevara et al. (2022b) this may be influenced by rate and boundary effects.

4. Calibration

The calibration method proposed in this paper requires both monotonic and cyclic tests, with the latter exploring differences in cyclic amplitude, load history and time for pore pressure dissipation. For this calibration exercise, three tests have been used with either a large number of constant amplitude cycles or multiple episodes of cycling, and three tests with increasing amplitude cycling. The tests were taken from two-way loading tests, although one-way loading tests were also performed in the centrifuge campaigns. Modelling of one-way loading tests using PICSI is discussed for one of these tests in the results section.

4.1. Calibration of the parallel-iwan model

For each soil type, embedment depth and test type (centrifuge or p-y apparatus) a monotonic push was performed. Each of these tests was used for the calibration of spring stiffness and slider capacity in the parallel-Iwan model, to then be used in its corresponding set of cyclic tests. Fig. 7 shows the measured monotonic backbone curves and the discretised PICSI backbone curves that were transformed into a parallel-Iwan system for each monotonic test performed in the centrifuge. Fig. 8 shows the same set of curves for the tests performed in the p-y apparatus. The number of parallel-Iwan elements used to model each monotonic

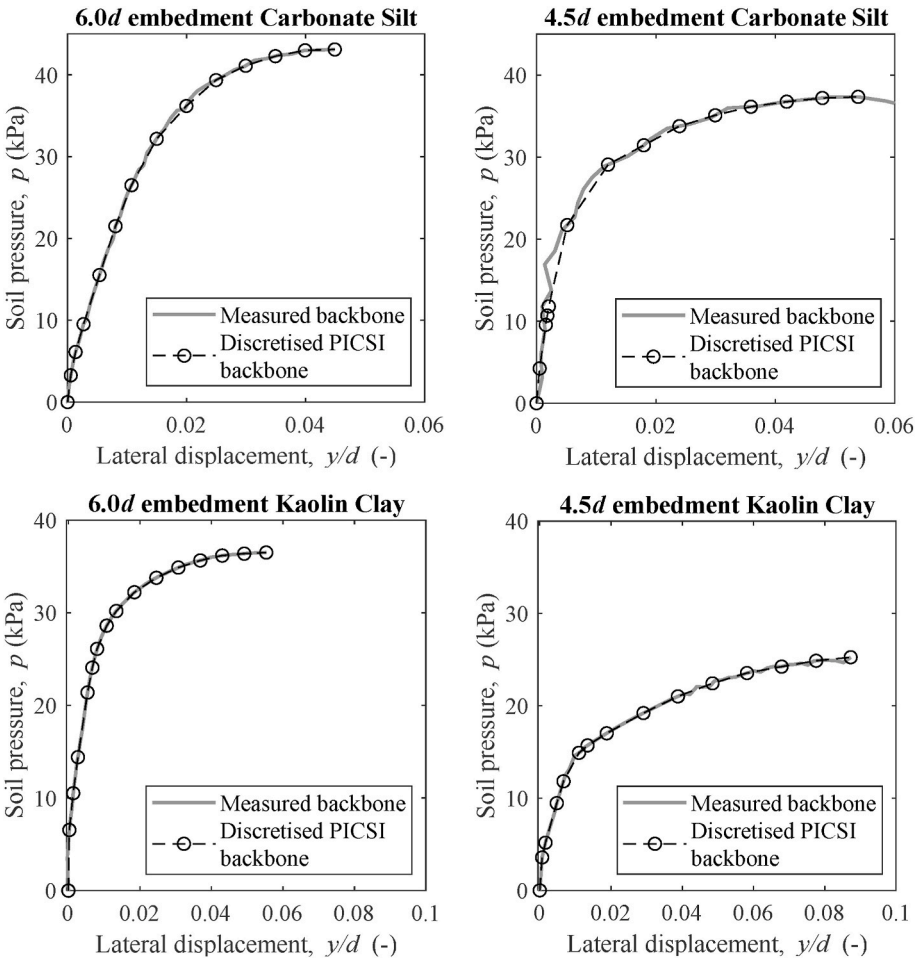

Fig. 7. Monotonic backbone curves from centrifuge tests discretised for PICSI.

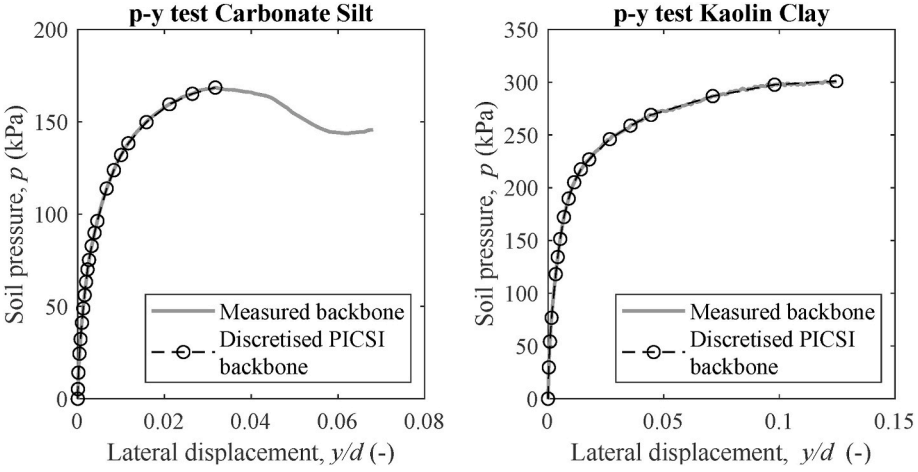

Fig. 8. Monotonic backbone curves from p-y apparatus discretised for PICSI.

test is shown in Table 5. The p-y curve is modelled up to the first peak, and any post-peak softening is not taken into account. Displacements beyond the peak at which the monotonic curve is modelled will mobilise the maximum pressure in the backbone curve minus the damage produced by the pore pressures accumulated up to that displacement. A current limitation of the model is that it does not include rate effects in its formulation, which is overcome in this study by performing all tests at a similar rate (roughly 1–3 mm/s at model scale).

4.2. Calibration of hardening and pore pressure dissipation parameters

The calibration procedure uses numerical optimisation, where an error function (E) was computed as the average normalised difference between the measured (K_{test}) and calculated (K_{PICSI}) secant stiffness values for each of the N cycles in a test (see Eq. (8)). To avoid an overweighting by tests with large number of cycles, the error was divided by the number of cycles (N) in the respective test. The

Table 5
Number of parallel-Iwan elements used to model each monotonic response.

Test number	Embedment Depth	Number of PI elements used
CS1	6.0 d	13
CS1	4.5 d	13
KC1	6.0 d	15
KC1	4.5 d	14
CS1_py	–	21
KC1_py	–	17

normalised errors were then summed up for all the tests used in the optimisation.

$$E = \left(\sum_{i=1}^{N} \frac{K_{test,i} - K_{PICSI,i}}{K_{test,i}} \right) \frac{1}{N} \quad (8)$$

The PatternSearch optimisation algorithm in Matlab (Mathworks, 2021) was used. The algorithm terminates when any of the following are satisfied.

- The change in the function value is less than a defined tolerance;
- The mesh size (or variation in the input parameters) is less than a defined tolerance; or
- The number of function evaluations reaches a defined number.

Fig. 9 illustrates of the optimisation process.

The list of PICSI parameters is given in Table 6. It was found to be more efficient to carry out parameter optimisation in two stages.

- In the first stage, the hardening parameters were assigned upper and lower bounds within plausible ranges, while the values of damage parameters were fixed to values from a previous manual fitting. Once the values for the consolidation and hardening parameters were selected, these were then constrained and the damage parameters optimised in the second stage.
- A second iteration was performed by fixing the optimised damage parameters and optimising the values for the consolidation and hardening parameters, then fixing the optimised consolidation and hardening parameters and optimising the damage ones. In total, five iterations were performed until the difference in the value of the parameters between iterations was negligible. The difference in the error function value between the first and last iteration was less than 1%, and the average error value on the last iteration for all the tests analysed was 21%.

Table 6
Calibrated PICSI model parameters for carbonate silt and kaolin clay.

Model feature	Description	Parameter	Carbonate silt	Kaolin clay
Strength limits	Slope of Damage = 0 line	λ^*	8.69	0.33
Damage generation	Rate constant	d_r	2.39	32.33
	Power constant	d_p	1.68	1.10
	Effect of amplitude	d_a	1.00	0.99
Pore pressure dissipation	Rate constant	c_r	0.30	0.05
	Power constant	c_p	9.65	5.00
Hardening	Slope of hardening path	κ^*	0.31	0.20
	Variation of hardening slope	h_p	0.002	0.010

The parameters λ^*, κ^*, c_p, c_r and h_p control strength and stiffness gain from hardening and consolidation, and can only be evaluated using tests

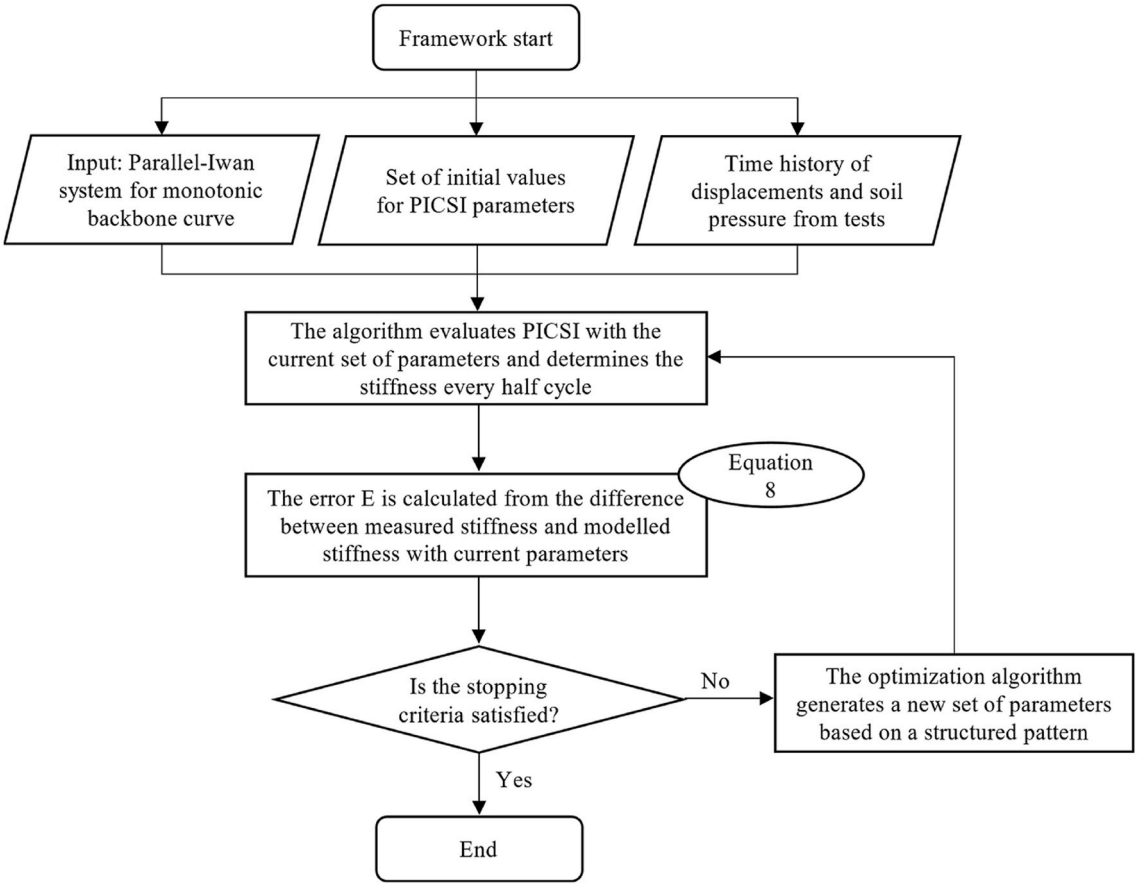

Fig. 9. Optimisation process flowchart.

where sufficient time was allowed to dissipate pore pressures. For the carbonate silt these parameters were therefore calibrated using tests CS5.2 and CS6 (which both have a large cyclic loading episode and consolidation periods), as well as test CS7 (which comprised a large single episode of 20,000 cycles). For the kaolin clay, test KC3 at both embedment depths and test KC4 were used to calibrate the hardening and consolidation parameters.

4.3. Damage parameters

The damage parameters (d_p, d_r, d_a) were calibrated using only the first episode of each test, during which the influence of pore pressure dissipation is minimal. Regarding the centrifuge tests, only the increasing amplitude phase of the first event of each test was used. As observed by Guevara et al. (2020, 2022a), once sufficient cycles at a large amplitude have occurred, the stiffness of subsequent smaller amplitude cycles may be impacted. This finding is clear in the centrifuge tests, where both shallow wedge and flow around mechanisms are mobilised; but is less evident in the p-y apparatus, where the stiffness of the subsequent smaller amplitude cycles appears to recover to the fully remoulded state observed before the large amplitude cycling occurred. This is thought to relate to differences in confinement of the upper portion of the soil in the p-y apparatus and the centrifuge tests - for the centrifuge tests, the near seabed the soil is free to deform in the vertical direction (without constraint from the soil above); whereas in the p-y apparatus, the soil is fully constrained above resulting in a deep flow around mechanism.

The tests selected for optimising the damage parameters for the carbonate silt were CS2 at 4.5 d and 6.0 d embedment and CS4_py, and the algorithm described in the previous section was used. For the kaolin clay, the tests used to optimise the damage parameters were KC2 and KC3 at 4.5 d embedment depth, and KC4_py.

4.4. Calibration results

Table 6 shows the optimised parameters for carbonate silt and kaolin clay obtained from the calibration procedure, which were then used to model the complete range of test loading sequence and compared directly to test results. Select results for carbonate silt are shown in Fig. 10, Figs. 11 and 12, while select results for kaolin clay are shown in Fig. 13.

Fig. 10 shows results of the two 10,000-cycles episodes single amplitude test CS7 (Table 2) alongside the PICSI model. The regain in secant stiffness from the model shows good agreement with the experimental data, including the sharp jump in stiffness after the pause period. However, the shape of the loading-unloading-reloading p-y loops is not accurately matched – the model does not include damping as part of its formulation, and therefore the shape of each loop is directly dependent on the monotonic response used to calibrate the parallel-Iwan spring system.

The ability of the model to predict multi-amplitude cyclic loading is shown in Fig. 11a, where results of a multi-amplitude test (CS2) at 4.5 d embedment are presented alongside the PICSI results. The secant stiffness from the PICSI model shows good agreement with the experimental data prior to the peak cyclic load, while the post peak behaviour is not accurately modelled – as discussed previously. In contrast, Fig. 11b shows that stiffness measured with the p-y apparatus (CS4_py) does return to a higher value for smaller amplitude cycling after a large amplitude cycling loading – and this is captured reasonably well by the PICSI model. The measured test data in the first packet of this test presents considerable scatter and lies around a value of K ≈ 3000–4000. It is possible that the accuracy of the p-y apparatus is not sufficient for these

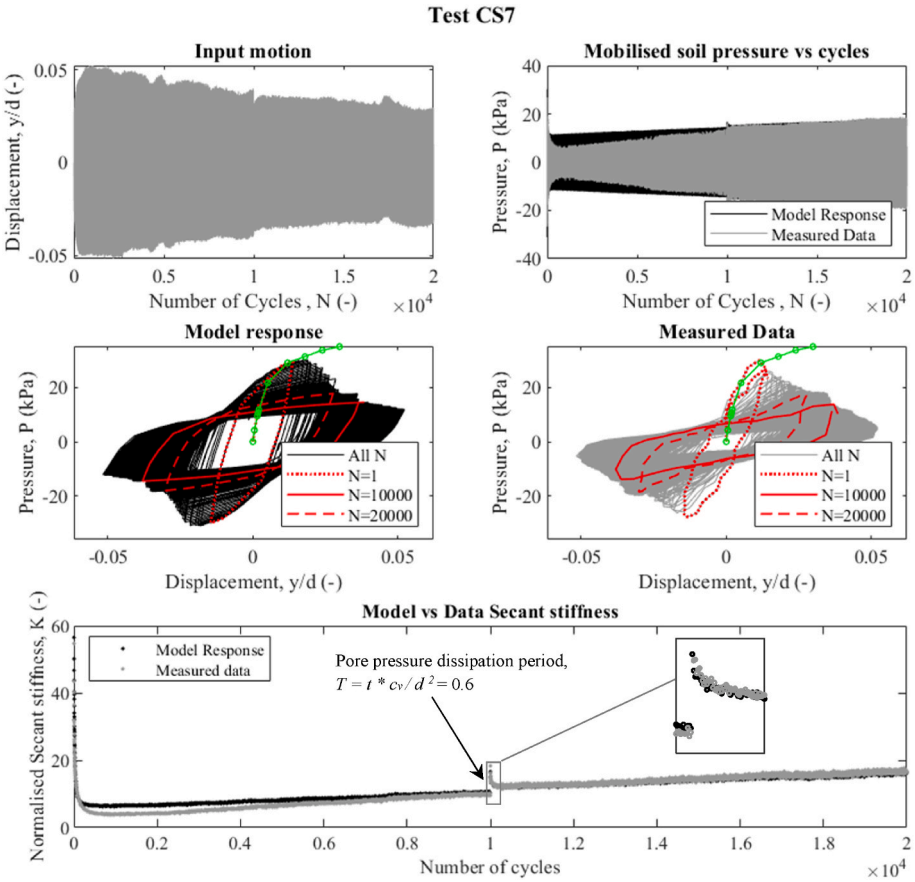

Fig. 10. Two-way centrifuge test on carbonate silt at 4.5D embedment depth: two episodes of 10,000 cycles single amplitude packets.

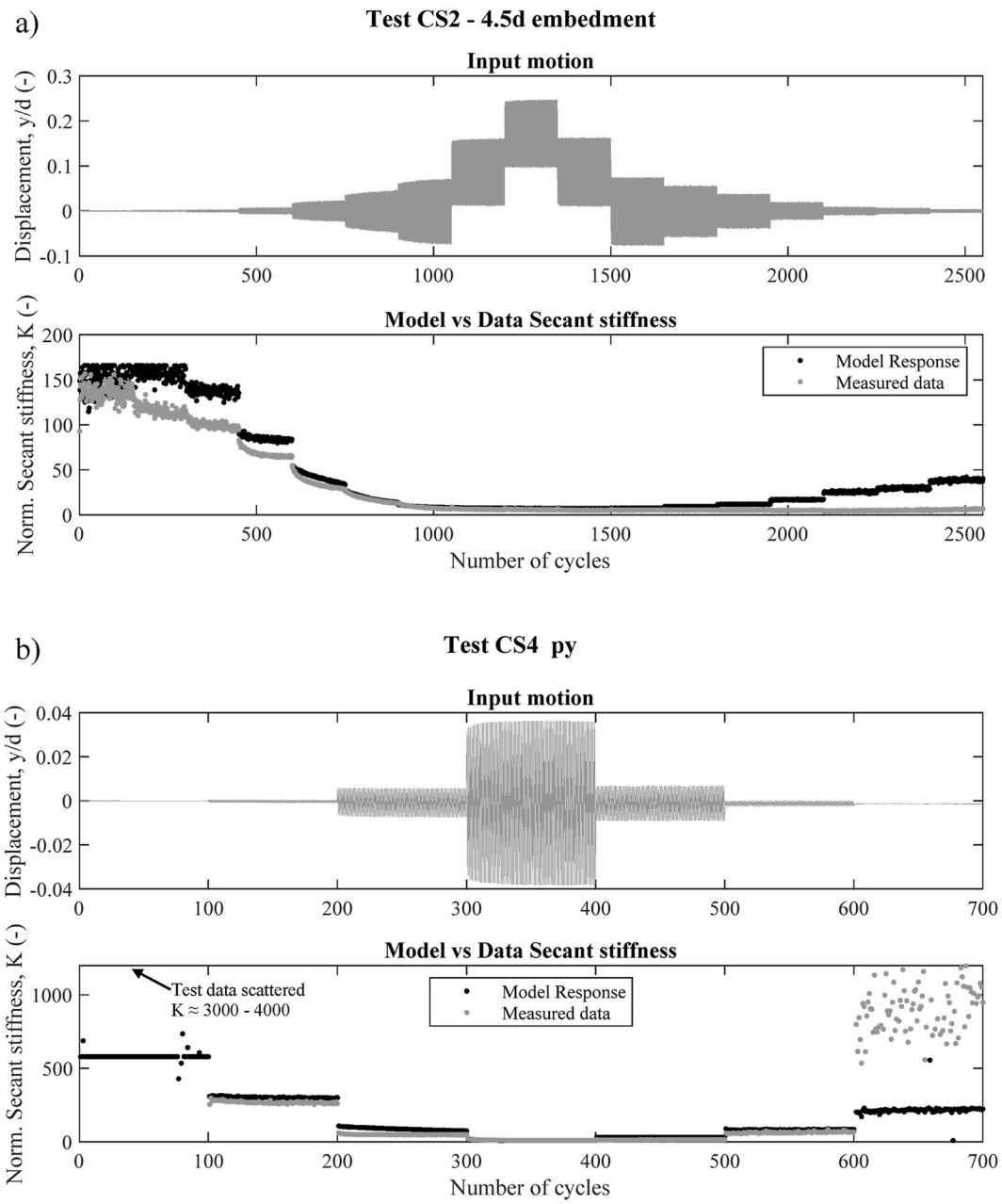

Fig. 11. Results of a) two-way centrifuge test on carbonate silt at 4.5D embedment depth: single episode of packets of increasing and decreasing amplitude, and b) two-way p-y apparatus test on carbonate silt: single episode of packets of increasing and decreasing amplitude.

smaller amplitudes (y/d ≈ 0.0005).

Fig. 12 presents the comparison for centrifuge test CS4 (embedded at 4.5 d) which comprised one-way multi-amplitude cyclic episodes with pore pressure dissipation periods. As observed in test CS2 (Fig. 11a), the post-peak stiffness does not return to its pre-peak value – although the PICSI model provides a good match up to this point.

The current formulation of PICSI does not capture scenarios where the pile translates into non-remoulded material, which is reflected in the experimental data (Fig. 12) as a tendency for the strength to return to the backbone curve when subjected to displacements larger than those experienced during cycling. While potentially important when designing for pile capacity, this is not expected to be significant for assessment of conductor fatigue as these analyses are conventionally performed considering no drift (i.e. 2-way loading).

For the kaolin clay, the PICSI model shows good agreement with the experimental p-y test data from test KC4_py from Fig. 13a, in terms of the changing normalised secant stiffness with cycles. The exception is for cycles 500 to 700, which are at very small displacements and the model does not seem to capture the return to a higher stiffness post-peak.

As observed before for Fig. 11b, it is possible that the accuracy of the p-y apparatus is not sufficient to capture the behaviour for smaller amplitudes (y/d ≈ 0.0005), which is why the data for the first and last packets in Fig. 13a presents considerable scatter.

The results of a multi-amplitude two-way test (KC3) at 4.5 d embedment are presented alongside the PICSI prediction are presented in Fig. 13b. From the figure it is observed that the secant stiffness from the PICSI model shows good agreement with the experimental data prior to the peak cyclic load, while the post peak behaviour is not accurately modelled. Nevertheless, the increase in stiffness due to cycling and reconsolidation prior to the peak in each cyclic event are observed in both the experimental data and the PICSI model.

Although some aspects of the behaviour are not properly captured in

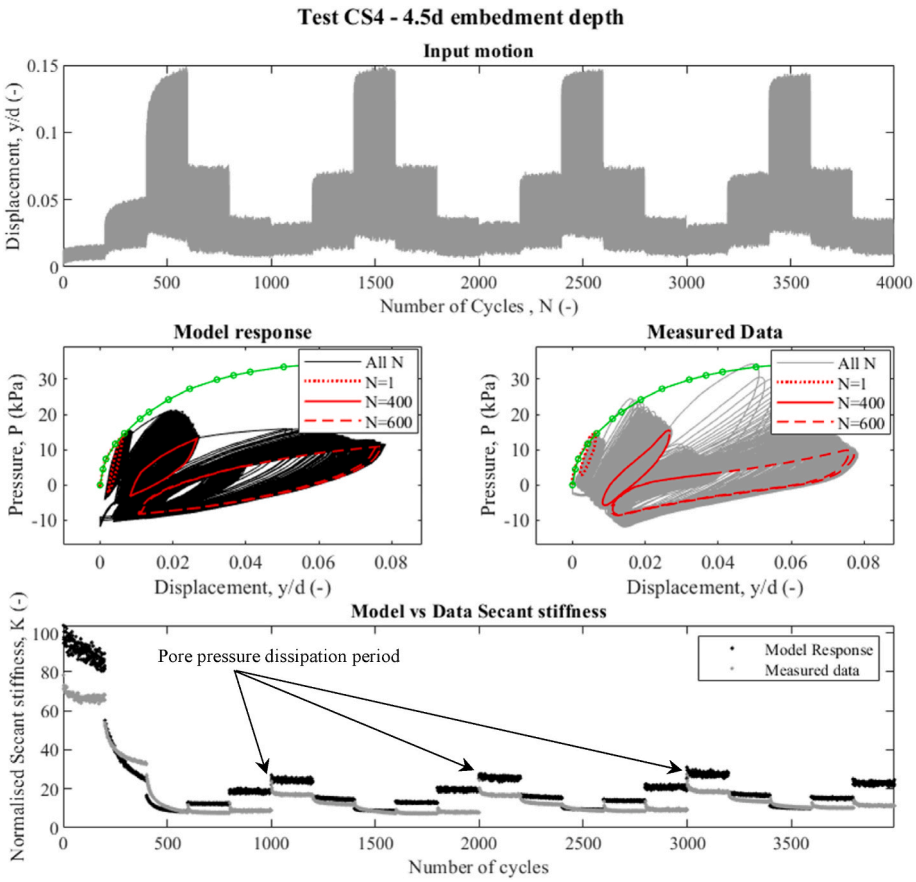

Fig. 12. One-way centrifuge test on carbonate silt at 4.5D embedment depth: four episode of packets of increasing and decreasing amplitude, with dissipation periods.

these comparisons, it is evident that the PICSI model captures the general observed trends of changing stiffness due to the competing processes of damage and reconsolidation, which is not possible using other p-y spring models.

5. Independent Validation

To validate the calibrated parameters for carbonate silt, results from a separate test performed in the centrifuge using a flexible pile were modelled using PICSI. Details of the experimental setup are given in Guevara et al. (2022a), with a summary of the prototype pile dimensions given in Table 7. The pile was instrumented with strain gauges along its length to measure changes in bending moments resulting from cyclic displacements imposed at the pile head. The imposed displacement sequence shown in Fig. 14.

The pile was modelled using the software LAP (Doherty, 2017). The pile-soil interface was assumed to be partially rough ($\alpha = 0.5$), with pile stiffness set equal to the measured value of 889 MN m^2 for the model. In the model, the soil strength gradient with depth was set at k = 1.66 kPa/m – determined by slow rate CK_0U simple shear tests, and consistent with T-bar tests performed in the sample. Measured sensitivity (from T-bar testing) was St = 5 in the centrifuge samples, with this value used in the PICSI model. The ultimate lateral soil pressure with depth (N_p. s_u) was determined using Jeanjean et al. (2017) assuming a no-gapping condition. The monotonic p-y curves were determined from simple shear tests using the scaling method proposed by Zhang and Andersen (2017), with scaling factors $\xi_e = 2.8$ and $\xi_p = 2.0$. The chosen value $\xi_p = 2.0$ is larger than recommended by Zhang and Andersen (2017), but this was selected in order to reduce the stiffness of the p-y curves at small strains, resulting in bending moment profiles that better match the first cycle of the test.

The monotonic backbone curve at each pile node was then transformed into a parallel-Iwan spring system. The cyclic pile head displacement sequence shown in Fig. 14 was then imposed at the pile head, with PICSI used to model the response of the soil at each time-step in the analysis. The results, in terms of head load throughout the test is shown in Fig. 15, and in terms of bending moment profiles for the first and last cycle of each packet of different amplitude of the test in Fig. 16. For comparison, the bending moment that would have been predicted using the monotonic curves that were input to PICSI is shown for each cyclic packet as the continuous grey line in Fig. 16. The results demonstrate that the calibrated PICSI model is able to capture changes in bending moment profile, including the load history effects on the stiffness. Key observations are as follows.

- The bending moment profile is relatively unchanged from cycle (N) = 1 to 400, which is attributed to the cyclic amplitude being sufficiently small to avoid 'damage' to the soil stiffness. However, once the amplitude increased (N = 401 to 600) there is a clear downward shift in the bending moment profile reflecting the loss of soil support close to the surface, which is well modelled by PICSI.
- The impact of the first large amplitude packet can be observed in the subsequent small amplitude sequence (N = 601 to 700) as a lower (and deeper) peak bending moment when compared to the previous low amplitude packet (N = 1 to 400). As noted earlier, at shallow depths PICSI is expected to overestimate the recovery of stiffness after larger amplitude cycling. The fact that the PICSI model matches the experimental data suggests that the level of non-recoverable softening in the soil wedge zone (where soil strength is lowest), as

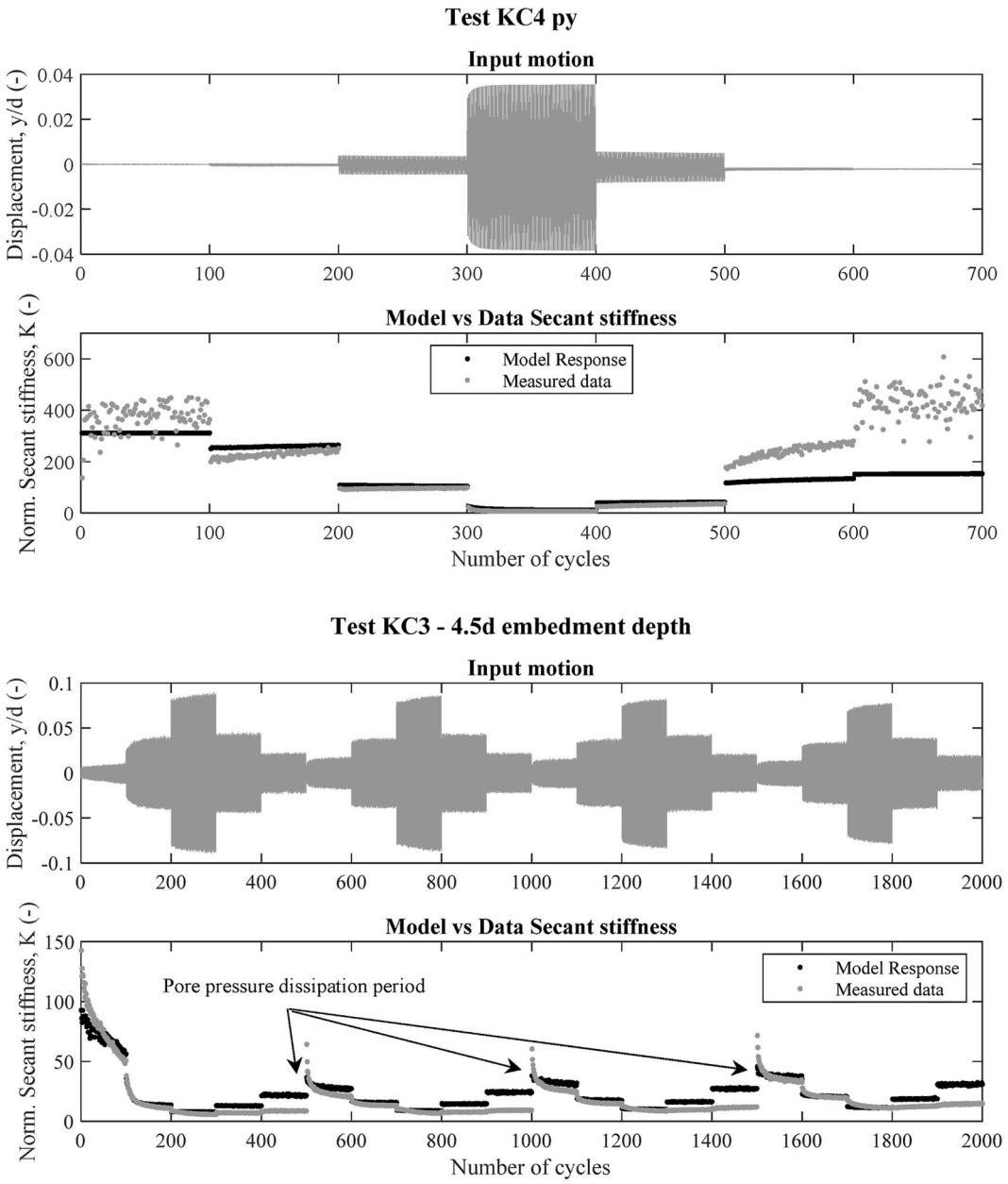

Fig. 13. Results of a) two-way p-y apparatus test on kaolin clay: single episode of packets of increasing and decreasing amplitude, and b) two-way centrifuge test on kaolin clay at 4.5D embedment depth: four episode of packets of increasing and decreasing amplitude, with dissipation periods.

Table 7
Test setup dimensions.

Dimension	Prototype at 80 g
Outer Diameter (Aluminium pile)	0.96 m
Wall thickness (Aluminium pile)	0.036 m
Wall coating (Aluminium pile + Epoxy coating)	0.0768 m
Total Outer Diameter	1.114 m
Embedment	18.24 m
Height of imposed displacement above mudline	3.36 m

created by higher amplitude cycling between N = 401 and 600, was insufficient to impact the bending moment profile.

- The shallow bending moment profile for N = 701 – the first cycle in the largest amplitude packet – is slightly underpredicted by PICSI soil springs, perhaps because the conductor is moving into fresh (undamaged) soil, which would result in an increase in resistance not captured by PICSI. However, the PICSI prediction accurately captures the peak BM, and is better than the estimate using the monotonic unsoftened profile (also shown). By N = 800 the experimental data and PICSI model prediction are in closer agreement.
- For N = 801 to 900 the bending moment profile predicted by the PICSI model is noticeably stiffer than suggested by the experimental data. This is consistent with PICSI overpredicting the recovery of stiffness (after high amplitude cycling) in the upper soil.

6. Discussion

Figs. 10–13 show that the model accurately captures the secant stiffness degradation and regain due to consolidation and hardening (except in post peak cycling and one-way loading conditions which will be discussed below), but does not accurately model the shape of the load-displacement loops. The area inside the loops (or damping) and how it changes with cycling could be significant for fatigue life

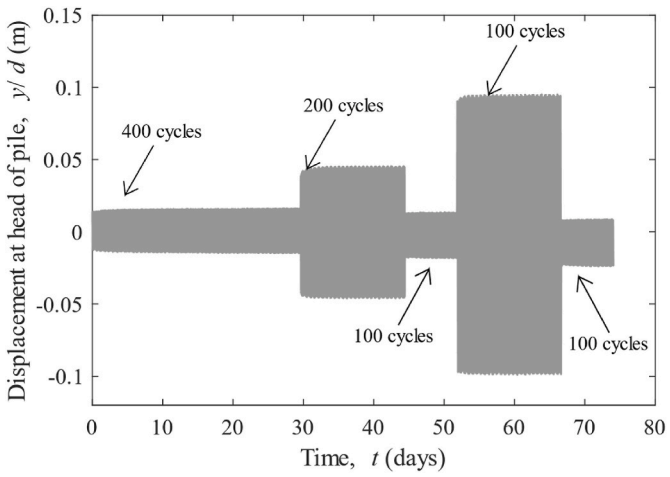

Fig. 14. Measured displacements at the pile head.

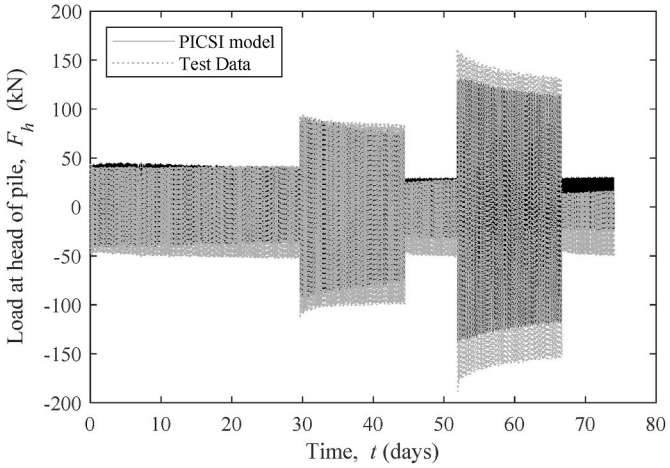

Fig. 15. Measured and modelled head load vs time.

estimation of conductors. The current study has not focussed on calibrating the hysteretic response and damping, but an approach to modify the Parallel-Iwan spring and slide capacities to better capture these effects could follow the same process as we have used for the other PICSI model parameters in this study. Our study has shown that bending moment evolution is better captured by our model thanks to the inclusion of time-varying stiffness effects, and it is reasonable to anticipate that our approach could also capture the hysteretic damping evolution as well or better than conventional methods.

It is observed that the post-peak secant stiffness cyclic degradation in the tests that had symmetric increasing and decreasing amplitude cycling (Figs. 11a, 12 and 13b) is not accurately modelled by PICSI. The post-peak behaviour shown by PICSI exhibits some recovery, consistent with that seen in the p-y apparatus test results shown in Figs. 11b and 13a. It is postulated that the upper soil surrounding the pile, where a wedge mechanism forms (like the rigid pile tests), degrades differently to the lower soil that flows around the pile (like the p-y apparatus tests). The reasons for this could be the lower confinement pressure near the soil surface, which allows the deformation with less constraint, or water entrainment during large amplitude cycling. A difference in degradation between wedge/flow failure mechanisms could explain why PICSI does not accurately predict the bending moment profile in the final cyclic packet from the flexible pile test (N = 801–900). In practice, this could be captured by using different PICSI model parameters for the deep failure mechanism (flow-around) and the shallow wedge, to reflect the different rates of softening and dissipation. Further refinement in the calibration could explore the possibility of obtaining two sets of parameters: one for the shallow wedge mechanism and another for the deep flow-around mechanism.

The current formulation of PICSI does not capture scenarios where the pile undergoes very high lateral displacement into non-remoulded material, which is reflected in the one-way test shown in Fig. 12, and in the first cycle of the large amplitude packet (N = 701) from the flexible pile test (Fig. 16). In the latter, the soil has experienced some damage due to the second cyclic amplitude packet (N = 401–600), before incursion into non-remoulded material in the first cycle of the fourth packet (N = 701–800). The bending moment profile of cycle 701 modelled by PICSI shows some degradation that is not observed in the experimental data. Nevertheless, by the end of the packet (N = 800), after the soil has remoulded, the PICSI model shows better agreement with the experimental data.

The advantage of PICSI is that it is able to model the changes in bending moments along the pile with different amplitude cycling. This is relevant for fatigue analysis of conductors, as the degradation of stiffness due to cycling will progressively shift the bending moments down the pile, inducing stresses in the lower components. Conversely, consolidation and hardening will shift the bending moments upwards, reducing the stresses in the lower components and increasing stresses in the upper sections of the conductor. The use of constant p-y curves throughout fatigue analysis are unable to model these shifts in stresses and if too stiff, may overestimate stress in the upper components of the conductor and underestimate them in the lower components (and vice versa if too soft).

7. Conclusions

This paper documents a calibration procedure for the Parallel-Iwan Critical State Inspired (PICSI) p-y model using data from rigid conductor physical model tests in the centrifuge and p-y apparatus. The method utilised an optimisation routine to determine the model parameters, rather than user judgement. Calibration of pore pressure dissipation (hardening) parameters were separated from calibration of the damage parameters.

As part of the calibration process, a simplification to the PICSI model is introduced that reduces the number of parameters to calibrate, that is achieved by assuming a linear envelope for the fully remoulded strength line (D = 1). This resulted in estimates that agree well with the experimental data.

The calibrated parameters were first compared to the complete set of rigid conductor tests, before being independently validated against experimental data using a flexible pile test. The later used a model based on PICSI generated springs distributed along the pile, which provided a good match to the cyclically induced changes in bending moment in the experiment. Future applications for fatigue assessment of conductors could implement either a decoupled model, such as the one presented in this paper, or introduce coded subroutines that support a coupled finite element model via updated springs at every timestep.

The rigid pile centrifuge tests used for the calibration represent mostly a shallow wedge failure mechanism, whereas the p-y apparatus tests represent a deep flow around failure mechanism. The combination of both for the calibration process provided a good match for the flexible pile data. Further refinement of the calibration could explore the possibility of obtaining two sets of parameters: one for the shallow wedge mechanism and another for the deep flow-around mechanism. Nevertheless, in the authors' opinion, centrifuge tests are currently the preferred method to calibrate the model, based on studies such as the present work, and current limitations of the p-y apparatus and its interpretation through episodic loading. In the long term it is desirable to widen the calibration routes, for example by improving the operation and interpretation of p-y-type lab apparatus, or by pursuing episodic cyclic simple shear tests and an interpretation route to link that data to p-y responses.

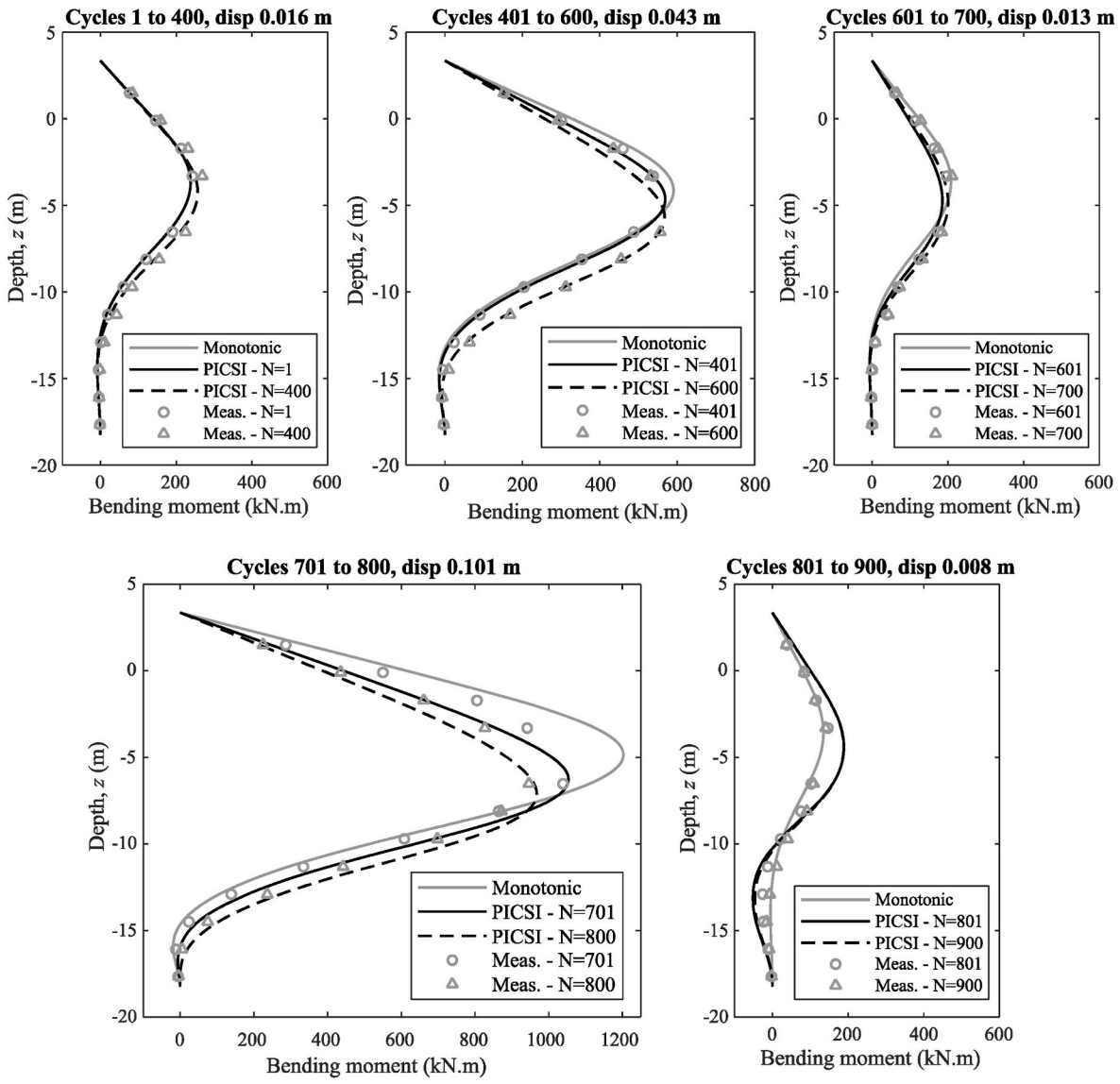

Fig. 16. Measured and modelled bending moment vs depth below mudline.

Future improvement of the PICSI model calibration process could explore the optimisation method proposed in this paper to calibrate the parameters for the PICSI model from monotonic and multiple episodic simple shear tests on other soil types. This would most likely involve scaling the stress-strain response from the simple shear tests to p-y curves, using methods already available in the literature.

CRediT authorship contribution statement

M. Guevara: Conceptualisation, Methodology, Software, Validation, Investigation, Data curation, Visualisation, Writing – original draft. **J.P. Doherty:** Conceptualisation, Methodology, Supervision, Software, Writing – review & editing. **P.G. Watson:** Conceptualisation, Writing – review & editing, Supervision, Funding acquisition. **D.J. White:** Methodology, Software, Writing – review & editing, Supervision, Funding acquisition.

Declaration of competing interest

The authors declare that they have no known competing financial interests or personal relationships that could have appeared to influence the work reported in this paper.

Data availability

Some of the data might be shared upon request.

Acknowledgements

The authors acknowledge the funding and execution of laboratory tests from the Norwegian Geotechnical Institute. The first author is supported by the ARC Industrial Transformation Research Hub for Offshore Floating Facilities which is funded by the Australian Research Council, Shell Australia, Woodside Energy, Bureau Veritas and Lloyd's Register (IH140100012). The third author leads the Shell Chair in Offshore Engineering research team at The University of Western Australia, which is sponsored by Shell Australia. The fourth author acknowledges the support of the EPSRC Offshore Renewable Energy Supergen Hub (EPSRC grant ref. EP/S000747/1).

References

API, 2014. Recommended Practice for Geotechnical and Foundation Design Considerations - API RP 2GEO. American Petroleum Institute.

Boukpeti, N., White, D.J., Randolph, M.F., Low, H.E., 2012. Strength of fine-grained soils at the solid-fluid transition. Geotechnique 62 (3), 213–226. https://doi.org/10.1680/geot.9.P.069.

Bransby, M.F., 1999. Selection of p-y curves for the design of single laterally loaded piles. Int. J. Numer. Anal. Methods GeoMech. 23 (15), 1909–1926.

Chow, S.H., O'Loughlin, C.D., Zhou, Z., White, D.J., Randolph, M.F., 2019. Penetrometer testing in a calcareous silt to explore changes in soil strength. Geotechnique 1–14.

DNV GL, 2019. DNVGL-RP-E104 Wellhead Fatigue Analysis. Edition 2019, Amended 2021.

Doherty, J., 2017. A web based application for the lateral analysis of pile (LAP) foundations. In: Proceedings of the ASME 2017 36th International Conference on Ocean, Offshore and Arctic Engineering, 9. Offshore Geotechnics. Trondheim, Norway: ASME.

Doherty, J., White, D.J., Watson, P.G., Grime, A., 2019. Life cycle changes in p-y stiffness for a conductor pile installed in carbonate silt. In: Proceedings of the 1st Vietnam Symposium on Advances in Offshore Engineering: VSOE 2018. Lecture Notes in Civil Engineering. Springer, Singapore, pp. 362–368.

Einav, I., Randolph, M.F., 2005. Combining upper bound and strain path methods for evaluating penetration resistance. Int. J. Numer. Methods Eng. 63 (14), 1991–2016. https://doi.org/10.1002/nme.1350.

Guevara, M., Doherty, J.P., Gaudin, C., Watson, P.G., 2022a. Evaluating uncertainty associated with engineering judgement in predicting the lateral response of conductors – a case study. J. Geotech. Geoenviron. Eng. https://doi.org/10.1061/(ASCE)GT.1943-5606.0002759.

Guevara, M., Doherty, J.P., Watson, P.G., White, D.J., 2020. Key features impacting soil-conductor lateral behaviour as illustrated by centrifuge tests. In: Proceedings of the 4th International Symposium on Frontiers in Offshore Geotechnics ISFOG 2020, pp. 1–10. Austin.

Guevara, M., Doherty, J.P., Watson, P.G., White, D.J., 2021. Evolving soil-conductor stiffness due to multiple-episode cyclic loading. In: Second Vietnam Symposium on Advances in Offshore Geotechnics. Ho Chi Minh City, pp. 1–8.

Guevara, M., Doherty, J., Watson, P., White, D., Boylan, N., Teng, Y., 2022b. A comparison study of soil-conductor stiffness from centrifuge and laboratory testing. In: Proceedings of the 20th International Conference on Soil Mechanics and Geotechnical Engineering. Sydney.

Hodder, M.S., White, D.J., Cassidy, M.J., 2009. Effect of remolding and reconsolidation on the touchdown stiffness of a steel catenary riser: observations from centrifuge modeling. In: Proceedings of the Annual Offshore Technology Conference. Houston. OTC-19871.

Hou, Z., 2020. Changing Soil Strength and Stiffness during Pipe-Soil Interaction at the Touch Down Zone. University of Western Australia.

ISO/DIS, 2021. ISO/CD 19901-4 Petroleum and Natural Gas Industries — Specific Requirements for Offshore Structures — Part 4 : Geotechnical Design Considerations. Under preparation, Geneva.

Iwan, W.D., 1966. A distributed-element model for hysteresis and its steady-state dynamic response. ASME. Journal of Applied Mechanics 33 (4), 893–900.

Jeanjean, P., 2009. Re-Assessment of P-Y Curves for Soft Clays from Centrifuge Testing and Finite Element Modeling. Offshore Technology Conference, Houston.

Jeanjean, P., Zhang, Y., Zakeri, A., Andersen, K.H., Gilbert, R., Senanayake, A., 2017. A framework for monotonic p-y curves in clay. In: Proceedings of the 8th International Conference of Offshore Site Investigation and Geotechnics, pp. 108–141. London.

Jostad, H.P., Carotenuto, P., Yusuke, S., 2021. Measuring and Modelling Cyclic Response of Dense Sand Under Partially Drained Conditions. In: Barla, M., Di Donna, A., Sterpi, D. (Eds.), Challenges and Innovations in Geomechanics. Springer International Publishing, Cham, pp. 447–455.

Komolafe, O., Aubeny, C., 2020. A p-y analysis of laterally loaded offshore-well conductors and piles installed in normally consolidated to lightly overconsolidated clays. J. Geotech. Geoenviron. Eng. 146 (6), 1–18.

Laham, N.I., Kwa, K.A., White, D.J., Gourvenec, S.M., 2021. Episodic simple shear tests to measure strength changes for whole-life geotechnical design. Géotech. Lett. 11 (1), 103–111. https://doi.org/10.1680/jgele.20.00124.

Mathworks, 2021. Global Optimisation Toolbox - Matlab. The Mathworks Inc, Natick, MA.

Osman, A.S., Randolph, M.F., 2012. Analytical solution for the consolidation around a laterally loaded pile. Int. J. GeoMech. 12 (3), 199–208.

Poulos, H.G., Hull, T., 1989. In: Kulhawy, F.H. (Ed.), The Role of Analytical Geomechanics in Foundation engineering." Foundation Engineering: Current Principles and Practice. ASCE, Reston, VA, USA, pp. 1578–1606.

Richardson, M.D., O'Loughlin, C.D., Randolph, M.F., Gaudin, C., 2009. Setup following installation of dynamic anchors in normally consolidated clay. J. Geotech. Geoenviron. Eng. 135 (4), 487–496.

Safaqah, O., Low, H.E., Pant, S., Ingarfield, S., Bransby, M.F., Randolph, M.F., Westgate, Z.J., 2022. Using penetrometer in situ and in box-core testing to obtain design information for lazy wave riser-soil interaction. In: Proceedings of the 5th International Symposium on Cone Penetration Testing (CPT'22). CRC Press, Bologna, pp. 214–219.

Sahdi, F., 2013. The Changing Strength of Clay and its Application to Offshore Pipeline Design. University of Western Australia.

Stewart, D., 1990. Lateral Loading of Piles in Soft Clay Due to Nearby Embankment Construction.

Stewart, D.P., Randolph, M.F., 1991. A new site investigation tool for the centrifuge. In: International Conference Centrifuge '91, pp. 531–538. Balkema, Rotterland.

White, D.J., Doherty, J.P., Guevara, M., Watson, P.G., 2022. A cyclic p-y model for the whole-life response of piles in soft clay. Comput. Geotech. 141, 104519 https://doi.org/10.1016/j.compgeo.20210104519, 1–11.

White, D.J., Hodder, M., 2010. A simple model for the effect on soil strength of episodes of remoulding and reconsolidation. Can. Geotech. J. 47 (7), 821–826.

Wood, D.M., 1990. Soil behaviour and critical state soil mechanics. In: Soil Behaviour and Critical State Soil Mechanics. Cambridge University Press.

Zakeri, A., Clukey, E.C., Kebadze, E.B., Jeanjean, P., 2016a. Fatigue analysis of offshore well conductors: Part I – study overview and evaluation of Series 1 centrifuge tests in normally consolidated to lightly over-consolidated kaolin clay. Appl. Ocean Res. 57, 78–95.

Zakeri, A., Clukey, E.C., Kebadze, E.B., Jeanjean, P., 2016b. Fatigue analysis of offshore well conductors: Part II – development of new approaches for conductor fatigue analysis in clays and sands. Appl. Ocean Res. 57, 96–113.

Zakeri, A., Sturm, H., Dyvik, R., Jeanjean, P., 2017. Development of novel apparatus to obtain soil resistance–displacement relationship for well conductor fatigue analysis. Can. Geotech. J. 54 (10), 1435–1446.

Zakeri, A., Sturm, H., Jeanjean, P., 2019. Validation and Extension of Soil Response Framework for Fatigue Analysis of Offshore Wells and Piles. Offshore Technology Conference (OTC 29236).

Zhang, D. White, Randolph, M., 2011. Centrifuge modeling of the cyclic lateral response of a rigid pile in soft clay. J. Geotech. Geoenviron. Eng. 137 (7), 717–729.

Zhang, Y., Andersen, K.H., 2017. Scaling of lateral pile p-y response in clay from laboratory stress-strain curves. Mar. Struct. 53, 124–135.

Zhang, Y., Andersen, K.H., Jeanjean, P., Mirdamadi, A., Gundersen, A.S., Jostad, H.P., 2017. A framework for cyclic p-y curves in clay and application to pile design in GoM. In: Offshore Site Investigation Geotechnics 8th International Conference Proceedings, S. For U. Technology, pp. 108–141. London.

Zhou, H., Randolph, M.F., 2009a. Numerical investigations into cycling of full-flow penetrometers in soft clay. Geotechnique 59 (10), 801–812. https://doi.org/10.1680/geot.7.00200.

Zhou, H., Randolph, M.F., 2009b. Resistance of full-flow penetrometers in rate-dependent and strain-softening clay. Geotechnique 59 (2), 79–86. https://doi.org/10.1680/geot.2007.00164.

Zhou, Z.F., 2019. The Changing Strength of Soft Soil Around Subsea Infrastructure. University of Western Australia.